AGU PUBLICATIONS

Radio Science

RESEARCH ARTICLE
10.1002/2017RS006471

Key Points:
- We formulate the system model and derive the log-likelihood ratio for a FM-based DP-MIMO radar system with antenna arrays
- We compute the analytically closed-form expressions of CRLB on the Cartesian coordinates of target position and velocity for DP-MIMO radar
- We find that increasing the number of receiving elements at each radar receiver can reduce the estimation errors

Supporting Information:
- Supporting Information S1
- Data Set S1

Correspondence to:
F. Wang,
wangxiaoxian@nuaa.edu.cn

Citation:
Shi, C. G., Wang, F., Salous, S., & Zhou, J. J. (2018). Cramér-Rao lower bounds for joint target parameter estimation in FM-based distributed passive radar network with antenna arrays. *Radio Science*, *53*, 314–333. https://doi.org/10.1002/2017RS006471

Received 11 OCT 2017
Accepted 21 DEC 2017
Accepted article online 31 JAN 2018
Published online 23 MAR 2018

Cramér-Rao Lower Bounds for Joint Target Parameter Estimation in FM-Based Distributed Passive Radar Network with Antenna Arrays

C. G. Shi[1], F. Wang[1], S. Salous[2], and J. J. Zhou[1]

[1]Key Laboratory of Radar Imaging and Microwave Photonics, Ministry of Education, Nanjing University of Aeronautics and Astronautics, Nanjing, China, [2]School of Engineering and Computing Sciences, Durham University, Durham, UK

Abstract To avoid the disadvantages of the active radar which utilizes its own transmitter to emit electromagnetic radiations, passive radars use the signals readily available in the environment and can provide superior capabilities of stealth target detection, low probability of intercept, low cost, and robustness. This paper investigates the joint target parameter (delay and Doppler) estimation performance for a frequency modulation (FM)-based distributed passive radar network (DPRN) system with antenna arrays. The DPRN system consists of multiple FM-based illuminators of opportunity and multiple radar receivers, which are placed on moving platforms. First, we consider the scenario where the target state parameters are unknown, the maximum likelihood estimator is developed, and the log-likelihood ratio of the received signal for a complex Gaussian extended target is derived. Then, the Cramér-Rao lower bounds (CRLBs) on the Cartesian coordinates of target position and velocity are computed for a DPRN system with M_T FM-based transmitters of Q antenna elements and M_R multichannel receivers of P antenna elements. Finally, numerical examples demonstrate that grouping the receiving antenna elements into properly sized arrays can reduce estimation errors. It is also shown that the joint CRLB is a function of signal-to-noise ratio, the number of receiving antenna elements, the properties of the transmitted FM waveform, and the relative geometry between the target and the DPRN architecture. The analytically closed-form expressions for CRLB are an important performance metric in that they enable the optimal placement of radar receivers to improve the target parameter estimation performance.

1. Introduction

1.1. Background and Motivation

In recent years, multiple-input multiple-output (MIMO) radar systems have attracted significant attention from the research community (Fisher et al., 2006; Li & Stoica, 2007, 2009; Niu et al., 2012). Different from the traditional phased array radar which only transmits scale versions of a single waveform (Hu et al., 2017), the MIMO radar can transmit uncorrelated waveforms from different transmitting antennas. These waveforms are separated and jointly processed by a set of matched filters in the multiple receivers. Generally, MIMO radars can be classified as distributed MIMO radar (Haimovich et al., 2008) and colocated MIMO radar (Li & Stoica, 2007). With widely separated transmit and receive antennas, the distributed MIMO radar, sometimes called multistatic radar system or radar networks (Naghsh et al., 2013; Niu et al., 2012), can view the target from different aspect angles, while all the transmit and receive antennas in the colocated MIMO radar are closely spaced, which only provides a single observation of the target. Hence, distributed radar network systems can provide enhanced target estimation capabilities by employing spatial diversity (Godrich et al., 2011).

Technically, parameter estimation performance can be assessed by Cramér-Rao lower bounds (CRLBs) on the estimation errors (Khomchuk et al., 2016), which can provide the smallest variance estimates for any unbiased estimation (Godrich et al., 2010; He, Blum, & Haimovich, 2010). Extensive research has been conducted into the derivations of CRLBs for distributed radar networks in various contexts such as target velocity estimation (He, Blum, Rodrich, & Haimovich, 2010), target location estimation (Godrich et al., 2010), noncoherent and coherent joint target position and velocity estimation (He, Blum, & Haimovich, 2010), and multiple-target joint parameter estimation (Wei et al., 2010). In (Kalkan, 2013), the CRLBs for the 2-D target localization and velocity estimations for widely separated MIMO radar are calculated, where the received signals are constructed by employing the Swerling target fluctuations to take into account the undesired effects of target amplitude

and phase fluctuations. In He et al. (2016), the authors derive the generalized CRLB for joint estimation of target position and velocity for distributed MIMO radar networks under more general conditions, such as the nonorthogonal signals, spatially dependent target reflection coefficients, and spatially dependent noise. This result is of high importance due to the fact that it describes the best achievable performance for some practical cases. The CRLBs of the joint time delay and Doppler shift estimation are derived in Zhao and Huang (2016) for an extended target, which analyzes the effects of transmitted waveform parameters on the estimation performance. Shi et al. (2016a) investigate the target parameter estimation performance of linear frequency modulation-based radar networks in a Rice fading environment. The numerical results suggest that the dominant scatterer component can be exploited to decrease the estimation errors, which is because the reception of dominant scatterer component increases the received signal-to-noise ratio (SNR) in the radar receiver. In Cheng et al. (2016), the CRLB for joint location and velocity estimation of moving target is calculated for distributed phased array radars, which are placed on moving platforms. It is also shown that increasing the signal bandwidth is beneficial to improve the location estimation accuracy, while the extended observation time can enhance the velocity estimation accuracy. Furthermore, the target parameter estimation performance is explored in Khomchuk et al. (2016) for a radar employing a set of widely separated transmitting and receiving antenna arrays, which considers multiple extended targets under stochastic and deterministic signal model assumptions. Overall, the previous studies lay a solid foundation for the problem of joint estimation of target location and velocity in multistatic radar systems.

1.2. Brief Survey of Similar Work

Since expensive transmission equipments are not required for passive radars, these systems can provide superior capabilities in many ways such as stealth target detection, low probability of intercept (Pace, 2009; Shi et al., 2015; Shi, Salous, et al., 2017; Shi, Wang, Sellathurai, et al., 2017; Shi, Zhou, & Wang, 2016; Zhang et al., 2015, 2016), low cost, and antijamming (Li, 1995). Passive radar is a type of bistatic radar, which utilizes the signals of opportunity as illuminators for target detection (Hack et al., 2014), parameter estimation (Zaimbashi, 2017), target tracking (Greco et al., 2011), and imaging (Daout et al., 2012). Furthermore, a passive radar system will offer spatial and signal diversities when it is deployed in a multistatic architecture, which is able to enhance its detection and estimation performance. In Filip and Shutin (2016), Gogineni et al. (2014), Javed et al. (2016), Shi, Wang, and Zhou (2016), Shi, Wang, Sellathurai, and Zhou (2016), Shi et al. (2016b), and Xie et al. (2017), the CRLB has been studied and applied to passive radar systems. The work in Shi, Wang, and Zhou (2016) presents the CRLB analysis for the joint target position and velocity estimation in a frequency modulation (FM)-based passive radar network, and it is indicated that more antennas mean better estimation performance. Due to the favorable ambiguity function properties and its wide deployment, the downlink signal of universal mobile telecommunications systems (UMTS) has been a potential illuminator of opportunity for a passive radar system. The modified CRLB (MCRLB) for UMTS-based passive radar networks is derived in Gogineni et al. (2014), where both noncoherent and coherent modes are considered. The MCRLB has been shown to offer a looser bound in practical applications, which can be employed as a good alternative to the classical CRLB due to the presence of random parameters in the transmitted signals (D'Andrea et al., 1994). In Javed et al. (2016), the results in Gogineni et al. (2014) are extended and the joint target parameter estimation performance of a UMTS-based passive multistatic radar is developed in a Rice fading environment, where it is demonstrated that the target estimation accuracy will be increased with an increase in reflection coefficient, number of transmitter-receiver pairs, the choice of the transmitter-receiver pairs, and duration time. Additionally, the MCRLB evaluation of an orthogonal frequency division multiplexing-based passive radar network can be found in Filip and Shutin (2016) and Shi, Salous, et al., 2016b). Two transmitter of opportunity subset selection schemes for FM-based passive radar network systems are proposed in Shi, Wang, Sellathurai, and Zhou (2016), which are formulated as knapsack problems and tackled with greedy selection approaches. Xie et al. (2017) investigate the problem of joint optimization of receiver placement and illuminator selection for a passive radar network.

1.3. Main Contributions

Overall speaking, this paper concentrates on the joint target position and velocity estimation performance of a FM-based distributed passive radar network (DPRN) system with antenna arrays. In such configuration, the multichannel radar receivers are placed on moving platforms, which is beneficial to find the optimal positions of radar receivers and obtain as low CRLBs as possible. The DPRN radar system can combine the advantages from spatial diversity, with the benefits of exploiting standard coherent array processing (Khomchuk et al., 2016). It is worth pointing out that almost all the research mentioned above consider

radars with widely distributed omnidirectional antennas and do not consider widely distributed transmitters/receivers with antenna arrays. For the DPRN system with antenna arrays placed on moving platforms, the things are much more complicated. To the best of our knowledge, the problem of joint target parameter estimation in FM-based DPRN system with antenna arrays, which has not been addressed until now, needs to be considered.

The major contributions of this work are threefold:

1. We formulate the system model and derive the log-likelihood ratio for a FM-based DPRN system with M_T FM-based transmitters of Q antenna elements and M_R radar receivers of P antenna elements. Note that references Filip and Shutin (2016), Gogineni et al. (2014), Javed et al. (2016), Kalkan, (2013), Shi, Wang, and Zhou (2016), and Shi et al. (2016a, 2016b) only evaluate the target parameter estimation performance for a multistatic radar system with widely distributed omnidirectional antennas and do not consider receive stations placed on moving platforms, while the authors in Kalkan (2013) and Khomchuk et al. (2016) concentrate on stationary platforms, and the DPRN system is ignored in Cheng et al. (2016) and Khomchuk et al. (2016). As an extension, this paper is a much more generalized case and quite different from the obtained results in Cheng et al. (2016), Filip and Shutin (2016), Gogineni et al. (2014), Javed et al. (2016), Kalkan, (2013), Khomchuk et al. (2016), Shi, Wang, and Zhou (2016), Shi et al. (2016a, 2016b), and Shi, Wang, Salous, and Zhou (2017).
2. We compute the analytically closed-form expressions of CRLB on the Cartesian coordinates of target position and velocity for a DPRN system, where it is assumed that each radar receiver is able to estimate and separate the scattered signals off the target due to different FM-based illuminators of opportunity with perfect accuracy. These expressions for MCRLB can be used as an important performance metric by aiding the optimal placement of radar receivers to improve the target parameter estimation accuracy.
3. With the aid of numerical simulations, we can find that increasing the number of receiving elements at each radar receiver can reduce the estimation errors. Previous results in Gogineni et al. (2014), Javed et al. (2016), and Shi, Wang, and Zhou (2016) only demonstrate that the CRLB is a function of the transmitted waveform parameters and the geometry between the target and the distributed MIMO radar configuration. In this paper, the effects of SNR and the number of receiving antenna elements on the joint target position and velocity estimation performance are also explored. To be specific, the joint CRLB is strongly dependent on the relative geometry between the target and the FM-based DPRN system, which incorporates the positions of the illuminators of opportunity, radar receivers, and target in the Cartesian space. On the other hand, it also depends on the number of receiving antenna elements at each receiver and the transmitted FM waveform such as observation time and modulation index.

The rest of this paper is organized as follows: The system model for the FM-based DPRN system is introduced in section 2.1, then the maximum likelihood estimation (MLE) of target parameters is presented in section 2.2. Section 3 derives the joint CRLB for analyzing the estimation performance. In section 4, several numerical examples and discussion are provided. Finally, the conclusion of this paper is given in section 5.

Notation: The superscript T denotes the transpose operator; $\mathbb{E}_{\mathbf{y}(t)|\boldsymbol{\mu}}\{\cdot\}$ denotes the expectation with respect to the distribution $p(\mathbf{y}(t)|\boldsymbol{\mu})$; $(\cdot)^*$ denotes the conjugation operators, respectively. $|\cdot|$ denotes the absolute value; $\Re\{\cdot\}$ is the real part, and $\Im\{\cdot\}$ is the imaginary part. The symbol $\nabla_{\theta}(\cdot)$ represents the gradient operator with respect to $\boldsymbol{\theta}$. $R_i(f)$ represents the Fourier transform of $r_i(t)$.

2. System Model and Estimation of Target Parameters

2.1. System Model

Consider a DPRN with M_T FM-based transmitters of opportunity and M_R multichannel radar receivers in a 2-D Cartesian space. Each transmitter and radar receiver consists of Q and P antenna elements, respectively. The center of the ith FM transmitter is located at $\overrightarrow{\mathbf{p}_i^t} = [x_i^t, y_i^t]$, $i = 1, \cdots, M_T$, while the center of the jth radar receiver is located at $\overrightarrow{\mathbf{p}_j^r} = [x_j^r, y_j^r]$, $j = 1, \cdots, M_R$. The low-pass equivalent waveform transmitted from the ith FM-based transmitter is $\sqrt{\frac{E_{\mathrm{FM}}}{M_T Q}} r_i(t)$, where E_{FM} denotes the total transmitted energy. The baseband signal corresponding to the ith transmitter $r_i(t)$ is normalized $\int_{-\infty}^{+\infty} |r_i(t)|^2 \mathrm{d}t = 1$, which is defined as follows:

$$r_i(t) = \begin{cases} \frac{1}{\sqrt{T_0}} e^{j\beta \sin(2\pi f t + \phi)}, & |t| \le \frac{T_0}{2}, \\ 0, & \text{elsewhere}, \end{cases} \tag{1}$$

where T_0 denotes the observation time, f denotes the instantaneous frequency, and ϕ is the signal phase (Shi et al., 2016). $\beta = \frac{\Delta f}{f}$ denotes the modulation index, where Δf denotes the maximum derivation of the instantaneous frequency f from the carrier frequency f_c. The modulation index indicates by how much the instantaneous frequency varies around its carrier frequency, which implies that larger modulation index leads to wider signal bandwidth. The baseband signals $r_i(t)$ are a set of unit energy waveforms which maintain approximately orthogonal for any time delay τ and Doppler shift f_D of interest (He, Blum, & Haimovich, 2010; Hu et al., 2017), such that $\int_{-\infty}^{+\infty} r_i(t) r_j^*(t-\tau) e^{j2\pi f_D t} dt$ equals 1 for $i = j$ and 0 for $i \neq j$. In this way, the signals from different FM transmitters can be separated at each radar receiver (He, Blum, & Haimovich, 2010).

Assume that a target is moving linearly and with constant velocity $\vec{\mathbf{v}} = [v_x, v_y]$ whose initial position is $\vec{\mathbf{p}} = [p_x, p_y]$, where $\vec{\mathbf{p}}$ and $\vec{\mathbf{v}}$ are supposed to be deterministic but unknown. The vector composed of all the unknown parameters is given by

$$\boldsymbol{\mu} = [p_x, p_y, v_x, v_y]^T. \tag{2}$$

Without loss of generality and to simplify the analysis, we consider the single-target case in this paper. However, the obtained results can be extended to the multiple-target scenario, in which the number of unknown parameters in the target state vector is increased by a factor equal to the number of targets.

In this paper, the multichannel radar receivers are placed on moving platforms. The jth receiver is moving with velocity $\vec{\mathbf{v}}_j^r = [v_{x,j}^r, v_{y,j}^r]$. Let $\tau_{ij}^{\boldsymbol{\mu}}$ and $f_{D_{ij}}^{\boldsymbol{\mu}}$ represent the bistatic time delays and Doppler shifts corresponding to the path between the ith FM transmitter, moving target, and the jth radar receiver:

$$\tau_{ij}^{\boldsymbol{\mu}} = \frac{\left\|\vec{\mathbf{p}} - \vec{\mathbf{p}}_i^t\right\| + \left\|\vec{\mathbf{p}} - \vec{\mathbf{p}}_j^r\right\|}{c_v}, \tag{3}$$

$$\begin{aligned} f_{D_{ij}}^{\boldsymbol{\mu}} = {} & \frac{1}{\lambda}\left[v_x\left(\frac{p_x - x_i^t}{\left\|\vec{\mathbf{p}} - \vec{\mathbf{p}}_i^t\right\|} + \frac{p_x - x_j^r}{\left\|\vec{\mathbf{p}} - \vec{\mathbf{p}}_j^r\right\|}\right)\right] + \frac{1}{\lambda}\left[v_y\left(\frac{p_y - y_i^t}{\left\|\vec{\mathbf{p}} - \vec{\mathbf{p}}_i^t\right\|} + \frac{p_y - y_j^r}{\left\|\vec{\mathbf{p}} - \vec{\mathbf{p}}_j^r\right\|}\right)\right] \\ & + \frac{1}{\lambda}\left[v_{x,j}^r \frac{p_x - x_j^r}{\left\|\vec{\mathbf{p}} - \vec{\mathbf{p}}_j^r\right\|} + v_{y,j}^r \frac{p_y - y_j^r}{\left\|\vec{\mathbf{p}} - \vec{\mathbf{p}}_j^r\right\|}\right], \end{aligned} \tag{4}$$

where c_v is the speed of light, λ denotes the carrier wavelength, $\left\|\vec{\mathbf{p}} - \vec{\mathbf{p}}_i^t\right\|$ denotes the distance from the ith transmitter to the target, and $\left\|\vec{\mathbf{p}} - \vec{\mathbf{p}}_j^r\right\|$ denotes the distance from the target to the jth receiver, respectively. One can notice from equations (3) and (4) that the time delay $\tau_{ij}^{\boldsymbol{\mu}}$ is a function of the unknown target position $\vec{\mathbf{p}} = [p_x, p_y]$, and the Doppler shift $f_{D_{ij}}^{\boldsymbol{\mu}}$ is a function of the unknown target position $\vec{\mathbf{p}} = [p_x, p_y]$ and velocity $\vec{\mathbf{v}} = [v_x, v_y]$.

2.2. Estimation of Target Parameters

Denote the signal received at the pth receiving antenna element of the jth radar receiver by $y_{jp}(t)$, which can be expressed as follows:

$$y_{jp}(t) = \sqrt{\frac{E_{\mathrm{FM}}}{M_T Q}} \sum_{i=1}^{M_T} \zeta_{ij} F r_i(t - \tau_{ij}^{\boldsymbol{\mu}}) e^{j2\pi f_{D_{ij}}^{\boldsymbol{\mu}} t} e^{j2\pi(p-1)\sin\theta_j^r D_R/\lambda} + n_{jp}(t), \tag{5}$$

where F is the transmitting antenna gain of the illuminator of opportunity, $\theta_j^r = \arctan[(y_j^r - p_y)/(x_j^r - p_x)]$, and D_R is the element spacing of radar receiver. $\zeta_{ij} = \zeta_{ijR} + j\zeta_{ijI}$ denotes the complex reflection coefficient corresponding to the ijth path, which is an unknown parameter. In a DPRN system, the FM-based transmitters of opportunity and radar receivers are sufficiently separated so that each transmitter-receiver path provides an independent aspect angle for the target, such that each of them has its own reflection coefficient. Thus, collect the target reflection coefficients for all transmitter-recevier paths in a column vector

$$\boldsymbol{\zeta} = [\zeta_{11}, \zeta_{21}, \cdots, \zeta_{N_t 1}, \zeta_{21}, \cdots, \zeta_{M_T M_R}]^T, \tag{6}$$

where ζ_{ij} is the target reflection coefficient corresponding to the ijth path which is supposed to be a complex Gaussian distributed variable with zero mean and covariance σ_ζ^2, that is, $\zeta_{ij} \sim \mathcal{CN}(0, \sigma_\zeta^2)$. Suppose that the target reflection coefficients for different paths are statistically independent for each other and remain

approximately constant over the observation period. It is also assumed that the target reflection coefficient ζ_{ij} is independent of the state vector $\boldsymbol{\mu}$ for $i = 1, \cdots, M_T$ and $j = 1, \cdots, M_R$. The term $n_{jp}(t)$ in (5) represents noise at the pth receiving antenna element of the jth radar receiver, which is supposed to be independent and identically distributed zero-mean complex Gaussian with variance σ_n^2, that is, $n_{jp} \sim \mathcal{CN}(0, \sigma_n^2)$. Note that the receiver noise $n_{jp}(t)$ for different jp are independent and that the target reflection coefficients and the noise are mutually independent.

The $P \times 1$ column vector which stacks all the observations of the jth radar receiver is (Cheng et al., 2016)

$$\mathbf{y}_j(t) = [y_{j1}(t), \cdots, y_{jp}(t), \cdots, y_{jP}(t)]^T. \tag{7}$$

The observations from all M_R receivers can be written as follows:

$$\mathbf{y}(t) = \left[\mathbf{y}_1^T(t), \cdots, \mathbf{y}_j^T(t), \cdots, \mathbf{y}_{M_R}^T(t)\right]^T, \tag{8}$$

which collects the observed signals from the entire set of the receiving antenna elements.

Under the assumptions mentioned before, the joint probability density function (PDF) of the received signals $\mathbf{y}(t)$ can be expressed as

$$p(\mathbf{y}(t)|\boldsymbol{\mu}, \boldsymbol{\zeta}) \propto \exp\left\{-\frac{1}{\sigma_n^2}\sum_{j=1}^{M_R}\sum_{p=1}^{P}\int_{-\infty}^{+\infty}\left|y_{jp}(t) - \sqrt{\frac{E_{\mathrm{FM}}}{M_T Q}}\sum_{i=1}^{M_T}\zeta_{ij}Fr_i\left(t-\tau_{ij}^{\boldsymbol{\mu}}\right)e^{j2\pi f_{D_{ij}}^{\boldsymbol{\mu}}t}e^{j2\pi(p-1)\sin\phi_j^r D_R/\lambda}\right|^2 \mathrm{d}t\right\}. \tag{9}$$

Furthermore, taking logarithm of the PDF in (9), we can obtain the log-likelihood ratio:

$$\begin{aligned}\Gamma(\mathbf{y}(t)|\boldsymbol{\mu}, \boldsymbol{\zeta}) &= \ln p(\mathbf{y}(t)|\boldsymbol{\mu}, \boldsymbol{\zeta}) \\ &= -\frac{1}{\sigma_n^2}\sum_{j=1}^{M_R}\sum_{p=1}^{P}\int_{-\infty}^{+\infty}\left|y_{jp}(t) - \sqrt{\frac{E_{\mathrm{FM}}}{M_T Q}}\sum_{i=1}^{M_T}\zeta_{ij}Fr_i\left(t-\tau_{ij}^{\boldsymbol{\mu}}\right)\right. \\ &\quad \left. e^{j2\pi f_{D_{ij}}^{\boldsymbol{\mu}}t}e^{j2\pi(p-1)\sin\phi_j^r D_R/\lambda}\right|^2 \mathrm{d}t + C,\end{aligned} \tag{10}$$

where C is a constant independent of the target state vector $\boldsymbol{\mu}$ and reflection vector $\boldsymbol{\zeta}$.

Due to the fact that the target reflection vactor $\boldsymbol{\zeta}$ is unknown, the log-likelihood ratio $\ln p(\mathbf{y}(t)|\boldsymbol{\mu})$ can be obtained by MLE. Specifically, the complex reflection coefficient of the ijth transmitter-receiver path maximizes $\Gamma(\mathbf{y}(t)|\boldsymbol{\mu}, \boldsymbol{\zeta})$ in (10), that is,

$$\begin{cases}\frac{\partial}{\partial\zeta_{ijR}}\Gamma(\mathbf{y}(t)|\boldsymbol{\mu}, \boldsymbol{\zeta})\Big|_{\zeta_{ijR}=\widehat{\zeta_{ijR}}} = 0, \\ \frac{\partial}{\partial\zeta_{ijI}}\Gamma(\mathbf{y}(t)|\boldsymbol{\mu}, \boldsymbol{\zeta})\Big|_{\zeta_{ijI}=\widehat{\zeta_{ijI}}} = 0.\end{cases} \tag{11}$$

Then, the maximum likelihood (ML) estimates of $\widehat{\zeta_{ijR}}$ and $\widehat{\zeta_{ijI}}$ are given by

$$\begin{cases}\widehat{\zeta_{ijR}} = \dfrac{\Re\left\{\sum_{p=1}^{P}\int_{-\infty}^{+\infty}y_{jp}(t)r_i^*\left(t-\tau_{ij}^{\boldsymbol{\mu}}\right)e^{-j2\pi f_{D_{ij}}^{\boldsymbol{\mu}}t}e^{-j2\pi(p-1)\sin\phi_j^r D_R/\lambda}\mathrm{d}t\right\}}{\sqrt{\frac{E_{\mathrm{FM}}}{M_T Q}}PF}, \\ \widehat{\zeta_{ijI}} = \dfrac{\Im\left\{\sum_{p=1}^{P}\int_{-\infty}^{+\infty}y_{jp}(t)r_i^*\left(t-\tau_{ij}^{\boldsymbol{\mu}}\right)e^{-j2\pi f_{D_{ij}}^{\boldsymbol{\mu}}t}e^{-j2\pi(p-1)\sin\phi_j^r D_R/\lambda}\mathrm{d}t\right\}}{\sqrt{\frac{E_{\mathrm{FM}}}{M_T Q}}PF}.\end{cases} \tag{12}$$

Hence, solving (11) to obtain $\widehat{\zeta_{ij}}$, the estimated target reflection coefficient corresponding to the ijth transmitter-receiver path can be written as

$$\widehat{\zeta_{ij}} = \widehat{\zeta_{ijR}} + j\widehat{\zeta_{ijI}} = \frac{\sum_{p=1}^{P}\int_{-\infty}^{+\infty}y_{jp}(t)r_i^*\left(t-\tau_{ij}^{\boldsymbol{\mu}}\right)e^{-j2\pi f_{D_{ij}}^{\boldsymbol{\mu}}t}e^{-j2\pi(p-1)\sin\phi_j^r D_R/\lambda}\mathrm{d}t}{\sqrt{\frac{E_{\mathrm{FM}}}{M_T Q}}PF}. \tag{13}$$

Substituting (13) into equation (10), then the log-likelihood ratio $\ln p(\mathbf{y}(t)|\boldsymbol{\mu})$ can be rewritten as

$$\begin{aligned}\Gamma(\mathbf{y}(t)|\boldsymbol{\mu}) &= \ln p(\mathbf{y}(t)|\boldsymbol{\mu}) \\ &= -\frac{1}{\sigma_n^2}\sum_{j=1}^{M_R}\sum_{p=1}^{P}\int_{-\infty}^{+\infty}\left|y_{jp}(t)\right|^2 \mathrm{d}t \\ &\quad + \frac{1}{P\sigma_n^2}\sum_{i=1}^{M_T}\sum_{j=1}^{M_R}\left|\sum_{p=1}^{P}\int_{-\infty}^{+\infty} y_{jp}(t) r_i^*\left(t-\tau_{ij}^{\boldsymbol{\mu}}\right) e^{-j2\pi f_{D_{ij}}^{\boldsymbol{\mu}} t} e^{-j2\pi(p-1)\sin\phi_j^r D_R/\lambda}\mathrm{d}t\right|^2.\end{aligned} \tag{14}$$

Subsequently, neglecting the constant term of the second line in (14), the estimate of the unknown target state vector $\boldsymbol{\mu}$ can be found as the minimizer of the function

$$\widehat{\boldsymbol{\mu}_{\mathrm{ML}}} = \arg\max_{\boldsymbol{\mu}} \Gamma(\mathbf{y}(t)|\boldsymbol{\mu}), \tag{15}$$

where $\widehat{\boldsymbol{\mu}_{\mathrm{ML}}}$ represents the MLE of the unknown parameter vector $\boldsymbol{\mu}$.

Remark 1: Note that a high dimensional search over the space consisting of the possible values of (p_x, p_y, v_x, v_y) is required for obtaining the ML estimate of $\boldsymbol{\mu}$ numerically, which may lead to large computational complexity. In addition, as the numbers of M_T, M_R, and P go up, the system complexity and computational load will be increased remarkably. In future work, we will explore some suboptimal methods to reduce computational complexity.

3. Joint Cramér-Rao Lower Bound

Using the system model and the MLE developed in the previous section, now we present the joint CRLB to estimate the target position (p_x, p_y) and velocity (v_x, v_y) for a DPRN system with M_T FM-based transmitters of Q antenna elements and M_R multichannel receivers of P antenna elements. It is indicated in Godrich et al. (2010) that the CRLB is a good prediction of the variance of the estimation error when SNR is large or the number of taken data samples is large. The first step in deriving CRLB is to compute the modified Fisher information matrix (FIM), which is a 4×4 matrix obtained from the second-order derivatives of the joint log-likelihood ratio (He, Blum, & Haimovich, 2010):

$$\begin{aligned}\mathbf{J}(\boldsymbol{\mu}) &= \mathbb{E}_{\mathbf{y}(t)|\mu}\left\{\nabla_{\mu}\Gamma(\mathbf{y}(t)|\boldsymbol{\mu})\left[\nabla_{\mu}\Gamma(\mathbf{y}(t)|\boldsymbol{\mu})\right]^T\right\} \\ &= -\mathbb{E}_{\mathbf{y}(t)|\mu}\left\{\nabla_{\mu}\left[\nabla_{\mu}\Gamma(\mathbf{y}(t)|\boldsymbol{\mu})\right]^T\right\}.\end{aligned} \tag{16}$$

Since $\Gamma(\mathbf{y}(t)|\boldsymbol{\mu})$ in (14) is a function of bistatic time delays and Doppler shifts, then we define a new parameter vector:

$$\boldsymbol{\Omega} = \left[\tau_{11}^{\boldsymbol{\mu}}, \tau_{12}^{\boldsymbol{\mu}}, \cdots, \tau_{M_TM_R}^{\boldsymbol{\mu}}, f_{D_{11}}^{\boldsymbol{\mu}}, f_{D_{12}}^{\boldsymbol{\mu}}, \cdots, f_{D_{M_TM_R}}^{\boldsymbol{\mu}}\right]^T, \tag{17}$$

which collects the unknown time delays and Doppler shifts corresponding to different transmit-receiver paths. According to the chain rule, the FIM can be given by

$$\mathbf{J}(\boldsymbol{\mu}) = \left(\nabla_{\mu}\boldsymbol{\Omega}^T\right)\mathbf{J}(\boldsymbol{\Omega})\left(\nabla_{\mu}\boldsymbol{\Omega}^T\right)^T, \tag{18}$$

where $\mathbf{J}(\boldsymbol{\Omega}) = -\mathbb{E}_{\mathbf{y}(t)|\boldsymbol{\Omega}}\{\nabla_{\boldsymbol{\Omega}}\Gamma(\mathbf{y}(t)|\boldsymbol{\Omega})[\nabla_{\boldsymbol{\Omega}}\Gamma(\mathbf{y}(t)|\boldsymbol{\Omega})]^T\}$.

Now we compute the term $\nabla_{\mu}\boldsymbol{\Omega}^T$. Recalling (2) and (17), $\nabla_{\mu}\boldsymbol{\Omega}^T$ can be obtained as follows:

$$\nabla_{\mu}\boldsymbol{\Omega}^T = \begin{bmatrix} \frac{\partial\tau_{11}^{\mu}}{\partial p_x} & \frac{\partial\tau_{12}^{\mu}}{\partial p_x} & \cdots & \frac{\partial\tau_{M_TM_R}^{\mu}}{\partial p_x} & \frac{\partial f_{D_{11}}^{\mu}}{\partial p_x} & \frac{\partial f_{D_{12}}^{\mu}}{\partial p_x} & \cdots & \frac{\partial f_{D_{M_TM_R}}^{\mu}}{\partial p_x} \\ \frac{\partial\tau_{11}^{\mu}}{\partial p_y} & \frac{\partial\tau_{12}^{\mu}}{\partial p_y} & \cdots & \frac{\partial\tau_{M_TM_R}^{\mu}}{\partial p_y} & \frac{\partial f_{D_{11}}^{\mu}}{\partial p_y} & \frac{\partial f_{D_{12}}^{\mu}}{\partial p_y} & \cdots & \frac{\partial f_{D_{M_TM_R}}^{\mu}}{\partial p_y} \\ 0 & 0 & \cdots & 0 & \frac{\partial f_{D_{11}}^{\mu}}{\partial v_x} & \frac{\partial f_{D_{12}}^{\mu}}{\partial v_x} & \cdots & \frac{\partial f_{D_{M_TM_R}}^{\mu}}{\partial v_x} \\ 0 & 0 & \cdots & 0 & \frac{\partial f_{D_{11}}^{\mu}}{\partial v_y} & \frac{\partial f_{D_{12}}^{\mu}}{\partial v_y} & \cdots & \frac{\partial f_{D_{M_TM_R}}^{\mu}}{\partial v_y} \end{bmatrix}, \tag{19}$$

where the entries of $\bigtriangledown_{\mu}\mathbf{\Omega}^{T}$ are provided:

$$\frac{\partial \tau_{ij}^{\mu}}{\partial x} \equiv \frac{1}{c_v}\left(\frac{p_x - x_i^t}{\left\|\vec{\mathbf{p}} - \vec{\mathbf{p}}_i^t\right\|} + \frac{p_x - x_j^r}{\left\|\vec{\mathbf{p}} - \vec{\mathbf{p}}_j^r\right\|}\right), \tag{20}$$

$$\frac{\partial \tau_{ij}^{\mu}}{\partial y} \equiv \frac{1}{c_v}\left(\frac{p_y - y_i^t}{\left\|\vec{\mathbf{p}} - \vec{\mathbf{p}}_i^t\right\|} + \frac{p_y - y_j^r}{\left\|\vec{\mathbf{p}} - \vec{\mathbf{p}}_j^r\right\|}\right), \tag{21}$$

$$\begin{aligned}\frac{\partial f_{D_{ij}}^{\mu}}{\partial x} \equiv \frac{1}{\lambda}\Bigg\{ & v_x\left[\frac{(p_y - y_i^t)^2}{\left\|\vec{\mathbf{p}} - \vec{\mathbf{p}}_i^t\right\|^3} + \frac{(p_y - y_j^r)^2}{\left\|\vec{\mathbf{p}} - \vec{\mathbf{p}}_j^r\right\|^3}\right] + v_y\left[-\frac{(p_x - x_i^t)(p_y - y_j^r)}{\left\|\vec{\mathbf{p}} - \vec{\mathbf{p}}_i^t\right\|^3} - \frac{(p_x - x_j^r)(p_y - y_j^r)}{\left\|\vec{\mathbf{p}} - \vec{\mathbf{p}}_j^r\right\|^3}\right] \\ & + \left[v_{x,j}^r \frac{(p_y - y_j^r)^2}{\|\vec{\mathbf{p}} - \vec{\mathbf{p}}_j^r\|^3} - v_{y,j}^r \frac{(p_x - x_j^r)(p_y - y_j^r)}{\|\vec{\mathbf{p}} - \vec{\mathbf{p}}_j^r\|^3}\right]\Bigg\},\end{aligned} \tag{22}$$

$$\begin{aligned}\frac{\partial f_{D_{ij}}^{\mu}}{\partial y} \equiv \frac{1}{\lambda}\Bigg\{ & v_x\left[-\frac{(p_x - x_i^t)(p_y - y_j^r)}{\left\|\vec{\mathbf{p}} - \vec{\mathbf{p}}_i^t\right\|^3} - \frac{(p_x - x_j^r)(p_y - y_j^r)}{\left\|\vec{\mathbf{p}} - \vec{\mathbf{p}}_j^r\right\|^3}\right] + v_y\left[\frac{(p_x - x_i^t)^2}{\left\|\vec{\mathbf{p}} - \vec{\mathbf{p}}_i^t\right\|^3} + \frac{(p_x - x_j^r)^2}{\left\|\vec{\mathbf{p}} - \vec{\mathbf{p}}_j^r\right\|^3}\right] \\ & + \left[-v_{x,j}^r \frac{(p_x - x_j^r)(p_y - y_j^r)}{\|\vec{\mathbf{p}} - \vec{\mathbf{p}}_j^r\|^3} + v_{y,j}^r \frac{(p_x - x_j^r)^2}{\|\vec{\mathbf{p}} - \vec{\mathbf{p}}_j^r\|^3}\right]\Bigg\},\end{aligned} \tag{23}$$

$$\frac{\partial \tau_{ij}^{\mu}}{\partial v_x} \equiv 0, \tag{24}$$

$$\frac{\partial \tau_{ij}^{\mu}}{\partial v_y} \equiv 0, \tag{25}$$

$$\frac{\partial f_{D_{ij}}^{\mu}}{\partial v_x} \equiv \frac{1}{\lambda}\left(\frac{p_x - x_i^t}{\left\|\vec{\mathbf{p}} - \vec{\mathbf{p}}_i^t\right\|} + \frac{p_x - x_j^r}{\left\|\vec{\mathbf{p}} - \vec{\mathbf{p}}_j^r\right\|}\right), \tag{26}$$

$$\frac{\partial f_{D_{ij}}^{\mu}}{\partial v_y} \equiv \frac{1}{\lambda}\left(\frac{p_y - y_i^t}{\left\|\vec{\mathbf{p}} - \vec{\mathbf{p}}_i^t\right\|} + \frac{p_y - y_j^r}{\left\|\vec{\mathbf{p}} - \vec{\mathbf{p}}_j^r\right\|}\right). \tag{27}$$

Next, we derive $\mathbf{J}(\mathbf{\Omega})$, which is a $2M_TM_R \times 2M_TM_R$ matrix. We can rewrite $\mathbf{J}(\mathbf{\Omega})$ in the form of a block matrix:

$$\mathbf{J}(\mathbf{\Omega}) = \begin{bmatrix} \mathbf{J}(\mathbf{\Omega})^{UL} & \mathbf{J}(\mathbf{\Omega})^{UR} \\ \mathbf{J}(\mathbf{\Omega})^{LL} & \mathbf{J}(\mathbf{\Omega})^{LR} \end{bmatrix}. \tag{28}$$

Based on the derivations in (Cheng et al., 2016; He, Blum, & Haimovich, 2010), we have

$$\begin{aligned}\mathbf{J}(\mathbf{\Omega})^{UL} &= \mathrm{diag}\left\{-\mathbb{E}_{\mathbf{y}(t)|\boldsymbol{\mu}}\left[\frac{\partial^2\Gamma(\mathbf{y}(t)|\mathbf{\Omega})}{\partial\left(\tau_{11}^{\mu}\right)^2}, \frac{\partial^2\Gamma(\mathbf{y}(t)|\boldsymbol{\mu})}{\partial\left(\tau_{12}^{\mu}\right)^2}, \cdots, \frac{\partial^2\Gamma(\mathbf{y}(t)|\boldsymbol{\mu})}{\partial\left(\tau_{M_TM_R}^{\mu}\right)^2}\right]\right\} \\ &= 8\pi^2\mathrm{diag}\left(\frac{PE_{\mathrm{FM}}F^2|\zeta_{11}|^2}{M_TQ\sigma_n^2}, \frac{PE_{\mathrm{FM}}F^2|\zeta_{12}|^2}{M_TQ\sigma_n^2}, \cdots, \frac{PE_{\mathrm{FM}}^2|\zeta_{M_TM_R}|^2}{M_TQ\sigma_n^2}\right) \\ &\odot \left\{\mathbf{I}_{M_R} \otimes \mathrm{diag}(\varepsilon_1, \varepsilon_2, \cdots, \varepsilon_{M_T})\right\},\end{aligned} \tag{29}$$

Table 1
Locations of FM-Based Transmitters of Opportunity

Transmitter	Position (m)
1	[2,000, 2,000]
2	[4,000, 1,000]
3	[3,000, 5,000]
4	[6,000, 3,000]

where $\mathbf{I}_{M_R}$ represents an $M_R \times M_R$ identity matrix, $\odot$ denotes the Hardmard product, $\otimes$ denotes the Kronecker product, and the term ε_i can be described by

$$\begin{aligned}\varepsilon_i &\equiv \int_{-\infty}^{+\infty} f^2 \left|R_i(f)\right|^2 \mathrm{d}f - \left|\int_{-\infty}^{+\infty} f \left|R_i(f)\right|^2 \mathrm{d}f\right|^2 \\ &= \frac{2\pi f \beta^2}{T_0}\left[2\pi f T_0 + \sin(2\pi f T_0)\cos(2\phi)\right].\end{aligned} \tag{30}$$

In a similar way, we can obtain

$$\begin{aligned}\mathbf{J}(\mathbf{\Omega})^{UR} &= \mathbf{J}(\mathbf{\Omega})^{LL} \\ &= \mathrm{diag}\left\{-\mathbb{E}_{\mathbf{y}(t)|\mathbf{\Omega}}\left[\frac{\partial^2 \Gamma(\mathbf{y}(t)|\boldsymbol{\mu})}{\partial \tau_{11}^{\mu} f_{D_{11}}^{\mu}}, \frac{\partial^2 \Gamma(\mathbf{y}(t)|\boldsymbol{\mu})}{\partial \tau_{12}^{\mu} f_{D_{12}}^{\mu}}, \cdots, \frac{\partial^2 \Gamma(\mathbf{y}(t)|\boldsymbol{\mu})}{\partial \tau_{M_T M_R}^{\mu} f_{D_{M_T M_R}}^{\mu}}\right]\right\} \\ &= 8\pi^2 \mathrm{diag}\left(\frac{PE_{\mathrm{FM}}F^2|\zeta_{11}|^2}{M_T Q \sigma_n^2}, \frac{PE_{\mathrm{FM}}F^2|\zeta_{12}|^2}{M_T Q \sigma_n^2}, \cdots, \frac{PE_{\mathrm{FM}}F^2|\zeta_{M_T M_R}|^2}{M_T Q \sigma_n^2}\right) \\ &\quad \odot \mathrm{diag}(\gamma_{11}, \gamma_{12}, \cdots, \gamma_{N_t N_r}),\end{aligned} \tag{31}$$

and

$$\begin{aligned}\mathbf{J}(\mathbf{\Omega})^{LR} &= \mathrm{diag}\left\{-\mathbb{E}_{\mathbf{y}(t)|\mathbf{\Omega}}\left[\frac{\partial^2 \Gamma(\mathbf{y}(t)|\boldsymbol{\mu})}{\partial \left(f_{D_{11}}^{\mu}\right)^2}, \frac{\partial^2 \Gamma(\mathbf{y}(t)|\boldsymbol{\mu})}{\partial \left(f_{D_{12}}^{\mu}\right)^2}, \cdots, \frac{\partial^2 \Gamma(\mathbf{y}(t)|\boldsymbol{\mu})}{\partial \left(f_{D_{M_T M_R}}^{\mu}\right)^2}\right]\right\} \\ &= 8\pi^2 \mathrm{diag}\left(\frac{PE_{\mathrm{FM}}F^2|\zeta_{11}|^2}{M_T Q \sigma_n^2}, \frac{PE_{\mathrm{FM}}F^2|\zeta_{12}|^2}{M_T Q \sigma_n^2}, \cdots, \frac{PE_{\mathrm{FM}}F^2|\zeta_{M_T M_R}|^2}{M_T Q \sigma_n^2}\right) \\ &\quad \odot \mathrm{diag}(\eta_{11}, \eta_{12}, \cdots, \eta_{M_T M_R}),\end{aligned} \tag{32}$$

where

$$\begin{aligned}\gamma_{ij} &\equiv \frac{1}{2\pi}\Im\left\{\int_{-\infty}^{+\infty} t r_i^*\left(t - \tau_{ij}^{\mu}\right)\frac{\partial r_i(t - \tau_{ij}^{\mu})}{\partial \tau_{ij}^{\mu}}\mathrm{d}t\right\} - \int_{-\infty}^{+\infty} f|R_i(f)|^2 \mathrm{d}f \int_{-\infty}^{+\infty} t\left|r_i\left(t - \tau_{ij}^{\mu}\right)\right|^2 \mathrm{d}t \\ &= \frac{\beta \sin(\phi)}{\pi f T_0}[\sin(\pi f T_0) - \pi f T_0 \cos(\pi f T_0)],\end{aligned} \tag{33}$$

$$\eta_{ij} \equiv \int_{-\infty}^{+\infty} t^2 \left|r_i\left(t - \tau_{ij}^{\mu}\right)\right|^2 \mathrm{d}f - \left|\int_{-\infty}^{+\infty} t\left|r_i\left(t - \tau_{ij}^{\mu}\right)\right|^2 \mathrm{d}t\right|^2 = \frac{T_0^2}{12}. \tag{34}$$

Remark 2: From equations (30), (33), and (34), one can observe that the terms ε_i, γ_{ij}, and η_{ij} are dependent on the characteristics of the transmitted FM signals. In section 4, some numerical examples will be presented to characterize the impacts of FM waveform parameters on the estimation performance.

Table 2
Locations and Velocities of Radar Receivers

Receiver	Position (m)	Velocity (m/s)
1	[1,000, 5,000]	[80, 20]
2	[0, 0]	[100, 100]
3	[4,000, 0]	[30, 50]

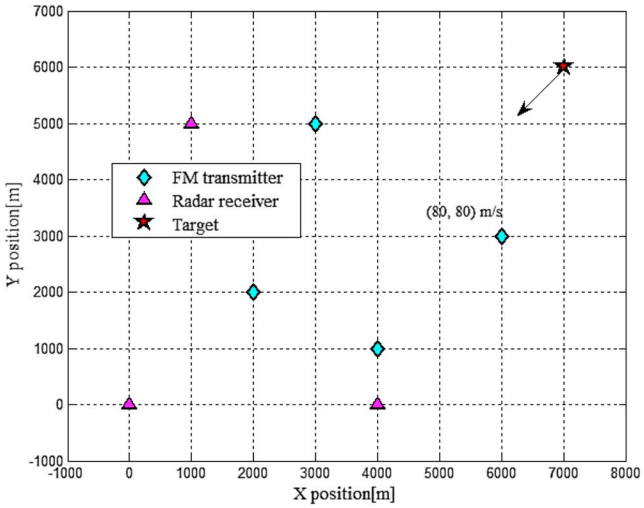

Figure 1. Simulated 2-D scenario with locations of frequency modulation-based transmitters of opportunity, multichannel radar receivers, and target.

After lengthy algebraic calculations, the final expression for joint FIM across all the transmitter-receiver paths can be written as follows:

$$\mathbf{J}(\boldsymbol{\mu}) = \sum_{i=1}^{M_T}\sum_{j=1}^{M_R} \frac{8\pi^2 P E_{\mathrm{FM}} F^2 |\zeta_{ij}|^2}{M_R Q \sigma_n^2} \mathbf{J}_{ij}(\boldsymbol{\mu}), \tag{35}$$

where the expressions for the elements of the bistatic FIM $\mathbf{J}_{ij}(\boldsymbol{\mu})$ corresponding to the ijth transmitter-receiver path are provided in Appendix A. The CRLB for the unknown target state vector $\boldsymbol{\mu}$ can be obtained by taking the inverse of the FIM in (35):

$$\mathrm{CRLB}(\boldsymbol{\mu}) = \mathbf{J}^{-1}(\boldsymbol{\mu}|\mathbf{c}). \tag{36}$$

Note that the FIM $\mathbf{J}(\boldsymbol{\mu})$ in (35) is a summation of $M_T M_R$ terms, such that each transmitter-receiver pair contributes information about the target's parameters of interest (Khomchuk et al., 2016). The joint CRLBs for the estimates of the unknown target position and velocity components can be determined by the diagonal elements of the inverse of the FIM evaluated at the true parameter value:

$$\begin{cases} \mathrm{var}(\hat{p}_x) \geq [\mathbf{J}^{-1}(\boldsymbol{\mu})]_{1,1}, \\ \mathrm{var}(\hat{p}_y) \geq [\mathbf{J}^{-1}(\boldsymbol{\mu})]_{2,2}, \\ \mathrm{var}(\hat{v}_x) \geq [\mathbf{J}^{-1}(\boldsymbol{\mu})]_{3,3}, \\ \mathrm{var}(\hat{v}_y) \geq [\mathbf{J}^{-1}(\boldsymbol{\mu})]_{4,4}, \end{cases} \tag{37}$$

where $\mathrm{var}(\hat{\varphi})$ denotes the variance of any unbiased estimation $\hat{\varphi}$ of the unknown parameter φ.

Remark 3: It is seen from (35) that the FIM depends on several factors. It is strongly dependent on the relative geometry between the target and the FM-based DPRN system, which incorporates the positions of the illuminators of opportunity, radar receivers, and target in the Cartesian space. Also, it depends on the number of receiving antenna elements at each receiver and the properties of the waveform such as observation time and modulation index. On the other hand, owing to the fact that the closed-form expression of $\mathbf{J}^{-1}(\boldsymbol{\mu})$ can be easily derived employing the chain rule, the CRLB can be computed for any nonsingular FIM. It should be noted that the computational complexity of the CRLB computation will be increased as we increase the numbers of transmit and receive stations, while the size of $\mathbf{J}(\boldsymbol{\mu})$ does not change with M_T and M_R (He, Blum, & Haimovich, 2010). In what follows, we present numerical simulations to compute the joint CRLB for a FM-based DPRN system with antenna arrays.

Remark 4: Since the standard CRLB provides optimistic predictions, it cannot be utilized for a realistic evaluation of the target parameter estimation performance in a surveillance scenario (Anastasio et al., 2014). The passive radar employing the illuminators of opportunity often operates with a low probability of detection for acceptable false alarm rates because of many reasons, for instance, the low transmit power, the transmitted waveform not designed for radar applications, and the wide antenna beams. For this reason, the CRLB with $P_{\mathrm{d}} < 1$ for joint target parameter estimation accuracy in a DPRN will be computed in future work.

4. Numerical Results and Discussion

In this section, some numerical and simulation results are provided to evaluate the previous theoretical findings (Data Set S1).

4.1. Numerical Description

Consider the FM-based DPRN system that has $M_T = 4$ stationary transmitters of opportunity and $M_R = 3$ radar receivers with known initial positions and velocities, which are shown in Tables 1 and 2, respectively. The carrier frequency of the transmitted FM signals is 100 MHz. Each transmitted signal has the observation time $T_0 = 0.5$ s, the modulation index $\beta = 5$, and the instantaneous frequency $f_c = 15$ KHz. The signal phase is set to be $\phi = \frac{\pi}{2}$. In order to compare different radar systems based on the same amount of transmitted energy and signal bandwidth, it is supposed that all FM-based illuminators of opportunity have single-element transmitting arrays, that is, $Q = 1$. The target moving with velocity [80, 80] m/s is assumed to be located at [7,000, 6,000] m. Without loss of generality and to simplify the analysis, we consider a scenario in a 2-D geometry as visualized in Figure 1. As mentioned before, the reflection coefficient corresponding to the ijth path ζ_{ij}

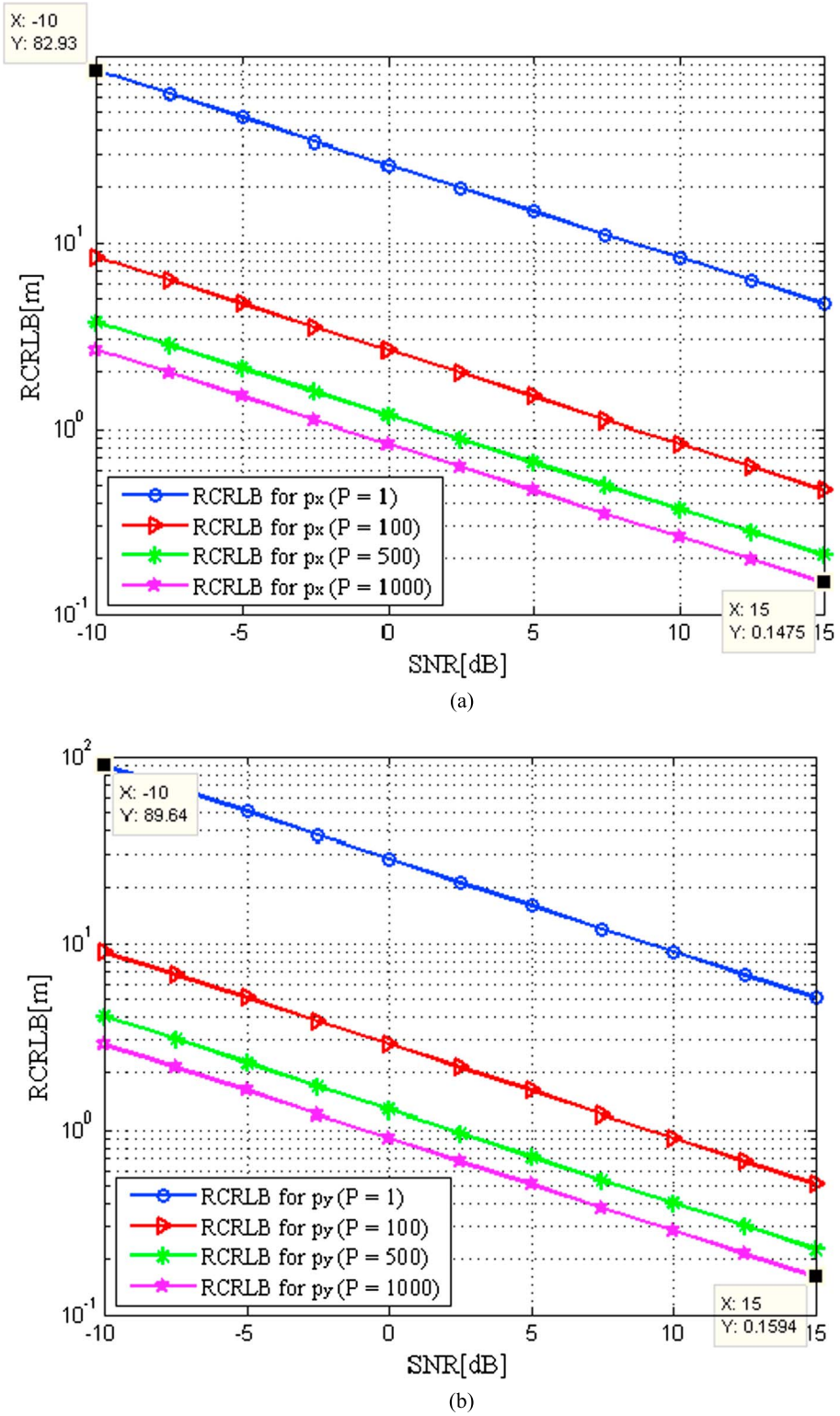

Figure 2. Square root of Cramér-Rao lower bound (RCRLB) in the target position dimensions versus signal-to-noise ratio (SNR) with different *P*: (a) *x* position; (b) *y* position.

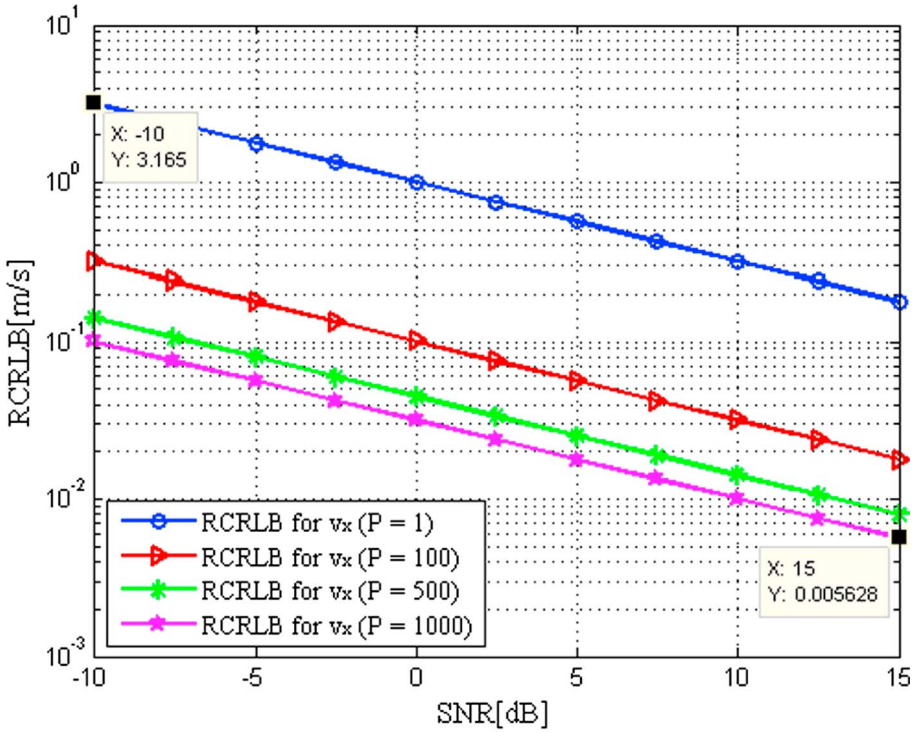

(a)

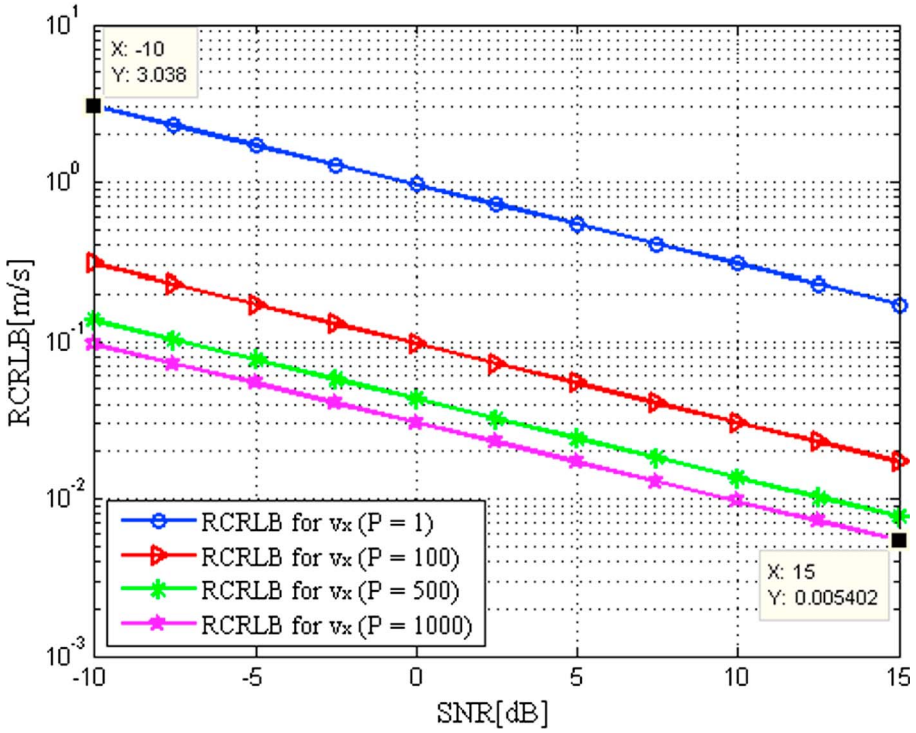

(b)

Figure 3. Square root of Cramér-Rao lower bound (RCRLB) in the target velocity dimensions versus signal-to-noise ratio (SNR) with different *P*: (a) *x* velocity; (b) *y* velocity.

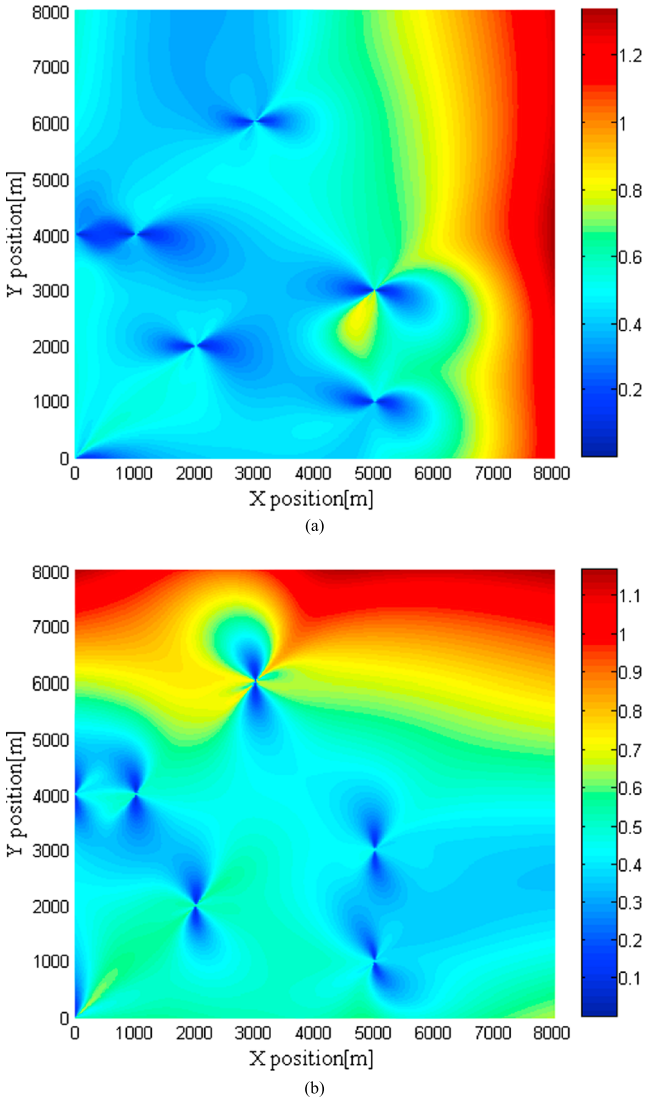

Figure 4. Square root of Cramér-Rao lower bound for target position dimensions in different position with SNR = 0 dB and $P = 1{,}000$: (a) x position; (b) y position.

is modeled as a zero-mean complex Gaussian random variable with variance $\sigma^2_{\zeta_{ij}}$, that is, $\zeta_{ij} \sim \mathcal{CN}(0, \sigma^2_{\zeta_{ij}})$. We define the SNR of the ijth transmitter-receiver path as

$$\mathrm{SNR}_{ij} = 10\lg\left(\frac{E_{\mathrm{FM}}F^2\sigma^2_{\zeta_{ij}}}{M_T Q\sigma_n^2}\right). \tag{38}$$

For simplicity, it is assumed that the different transmit-to-receive array paths have the same variance σ^2_ζ, so that the SNRs corresponding to different ij paths are the same, that is, $\mathrm{SNR} = \mathrm{SNR}_{ij}$.

4.2. Numerical Results

Figures 2 and 3 illustrate the noncoherent square roots of CRLBs (RCRLBs) of target position and velocity versus SNR, respectively. In both figures, we can observe that the RCRLBs for target position and velocity estimates are reduced as the SNR value goes up. It is also seen that the curves for $P = 1$ are much higher than the ones for $P = 1{,}000$, indicating that a larger number of receiving antenna elements leads to better target estimation accuracy, as expected. Obviously, the case with $P = 1$ yields the worst target estimation performance, which implies the advantage of utilizing multiple receiving antenna elements.

Next, we employ the RCRLBs of target position and velocity estimations to investigate the effects of the relative geometry between the target and the linear frequency modulation-based distributed MIMO radar

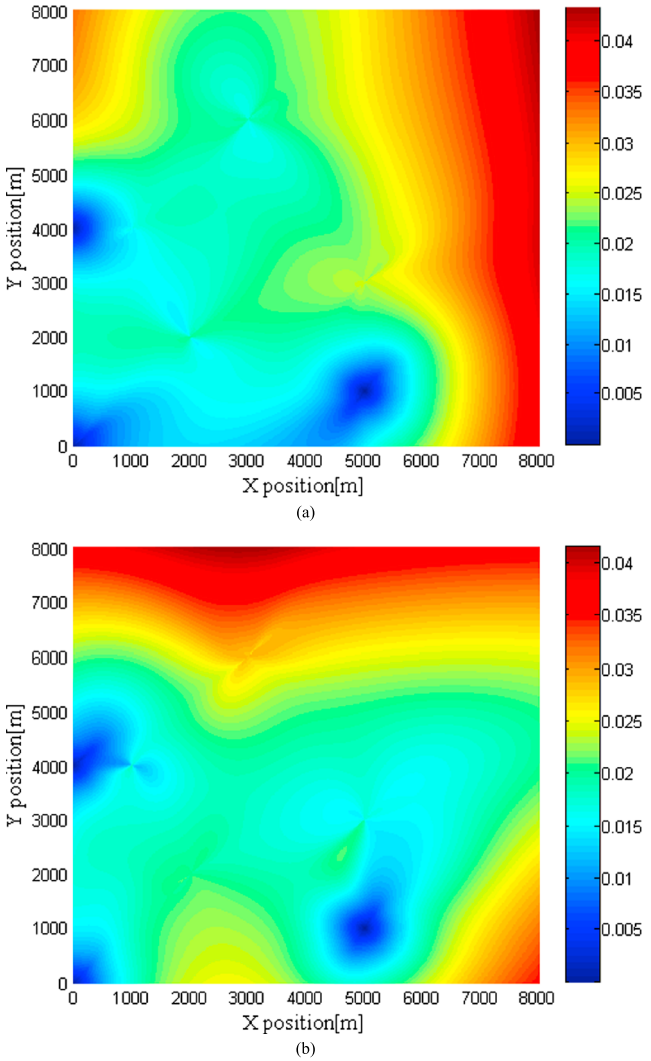

Figure 5. Square root of Cramér-Rao lower bound for target velocity dimensions in different position with SNR = 0 dB and P = 1,000: (a) x velocity; (b) y velocity.

configuration on the target estimation performance. Figures 4 and 5 depict the RCRLBs for both target position and velocity in different position with fixed SNR=10 dB and P= 1,000. From these figures, we can find that the target parameter estimation performance implied by the RCRLBs on the Cartesian coordinates of target position and velocity are different when the target is placed at different locations. In other words, as the relative geometry between the target and the DPRN architecture changes by changing the target location, the RCRLB values are changed. This is because the geometry between the target and the DPRN system impacts the derivatives of the delay-Doppler terms with respect to the Cartesian coordinates remarkably (Shi et al., 2016a, 2016b), which supports the correctness of the CRLB derivation in section 3. These results will open up a new dimension for DPRN system by aiding the optimal placement of multichannel radar receivers to improve the target parameter estimation accuracy.

In Figures 6 and 7, for a fixed T_0 = 1 s, the RCRLBs for both target position and velocity estimates are plotted versus the SNR value. It is observed that the RCRLBs decrease with the increase of observation time T_0. In particular, in Figure 2, at an SNR of 15 dB, the RCRLBs for the x and y positions are 0.1475 m and 0.1594 m when P = 1,000, respectively. In Figure 3, the RCRLBs for the x and y velocities are 0.005628 m/s and 0.005402 m/s when SNR = 15 dB and P = 1,000, respectively, while the results in Figure 6 show that the RCRLB at SNR = 15 dB for p_x is 0.1273 m and that for p_y is 0.1358 m. In Figure 7, the RCRLB at SNR = 15 dB for v_x is 0.003307 m/s and that for v_y is 0.003105 m/s.

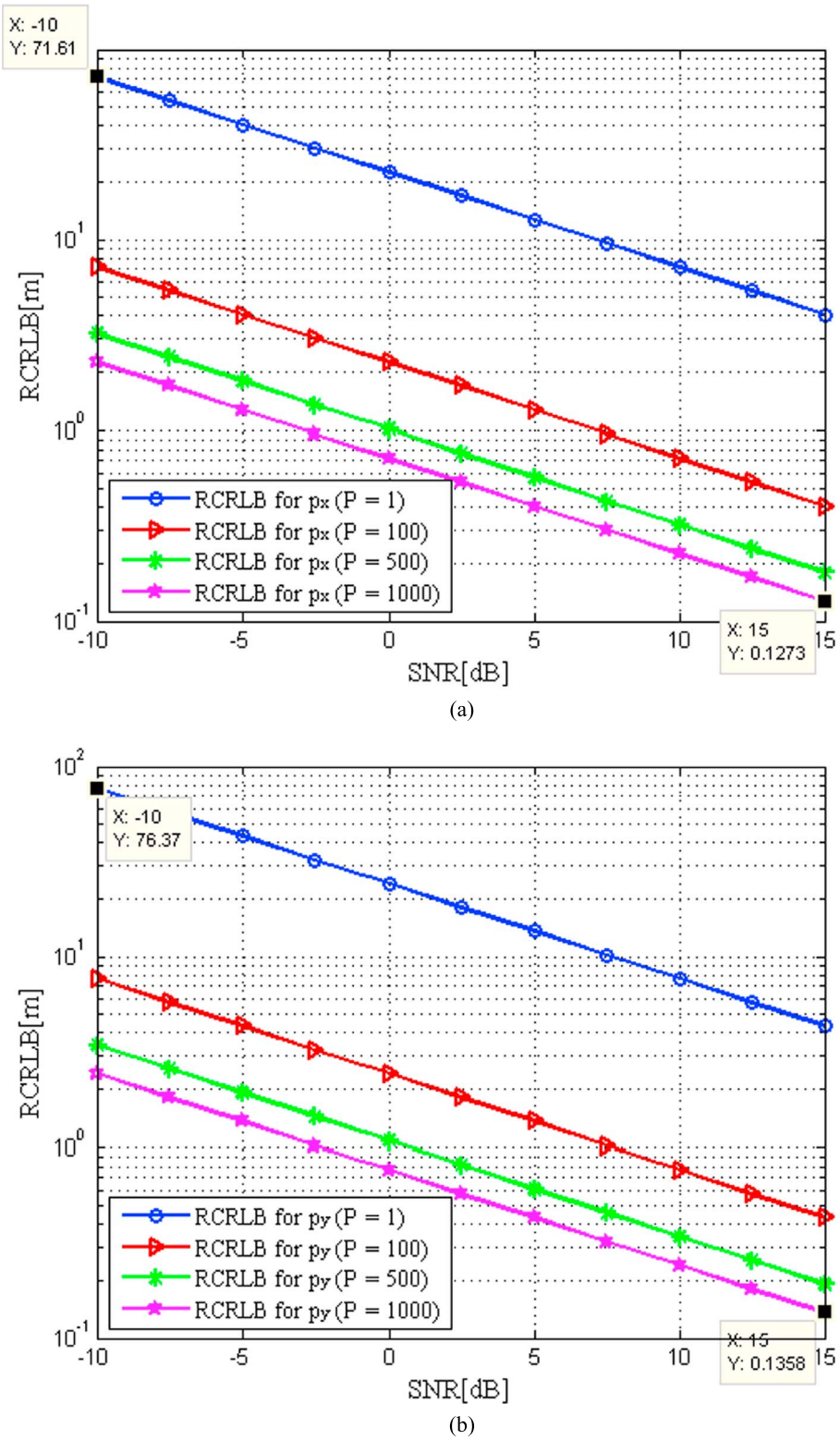

Figure 6. Square root of Cramér-Rao lower bound (RCRLB) in the target position dimensions versus signal-to-noise ratio (SNR) with different P when $T_0 = 1$ s: (a) x position; (b) y position.

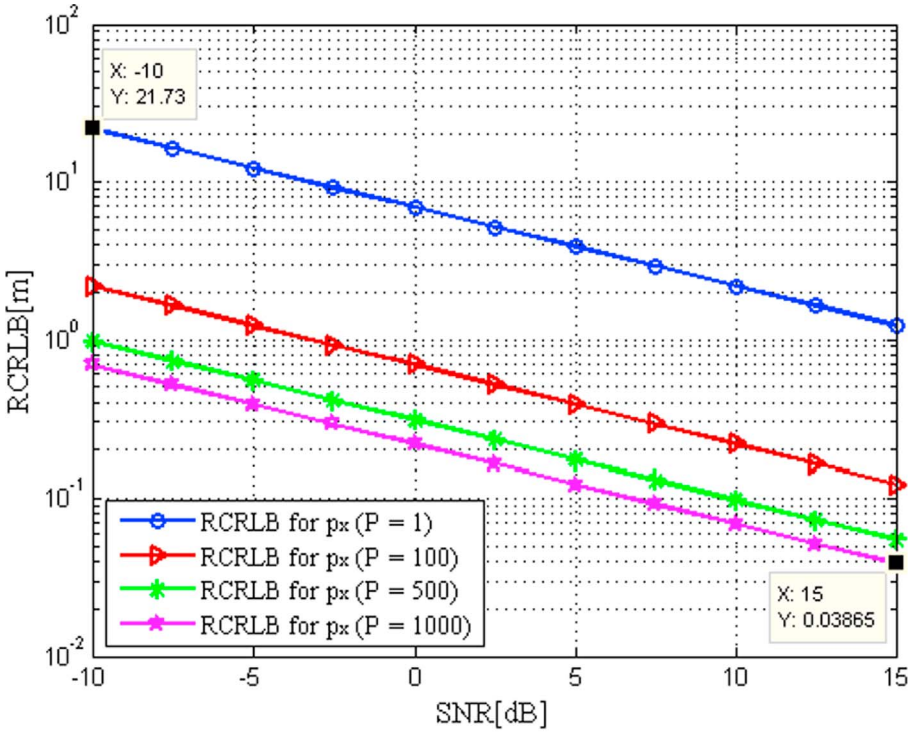

(a)

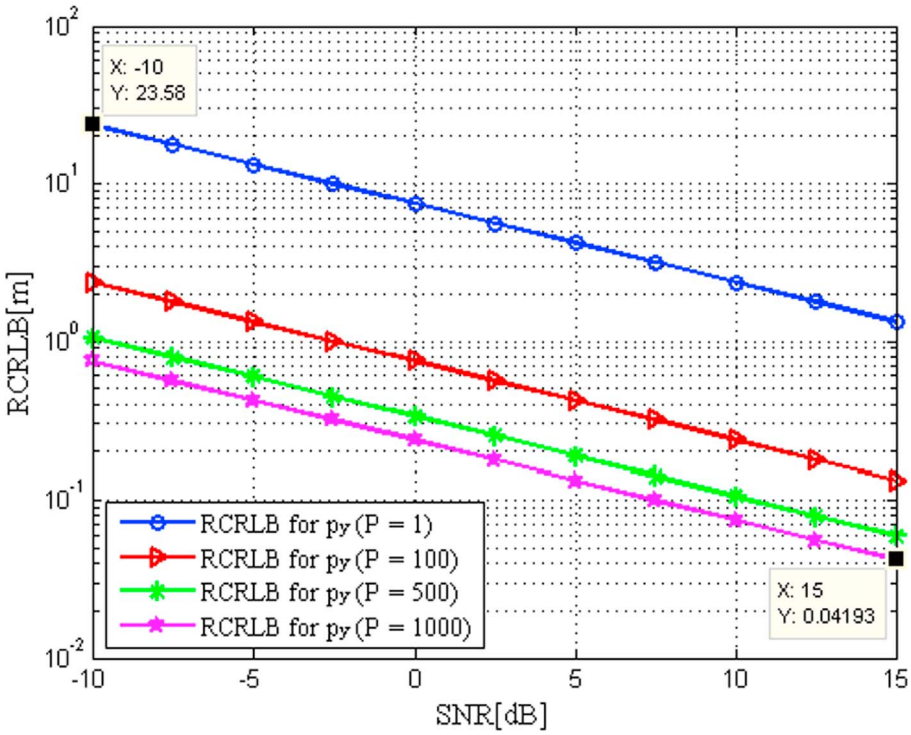

(b)

Figure 7. Square root of Cramér-Rao lower bound (RCRLB) in the target velocity dimensions versus signal-to-noise ratio (SNR) with different P when $T_0 = 1$ s: (a) x velocity; (b) y velocity.

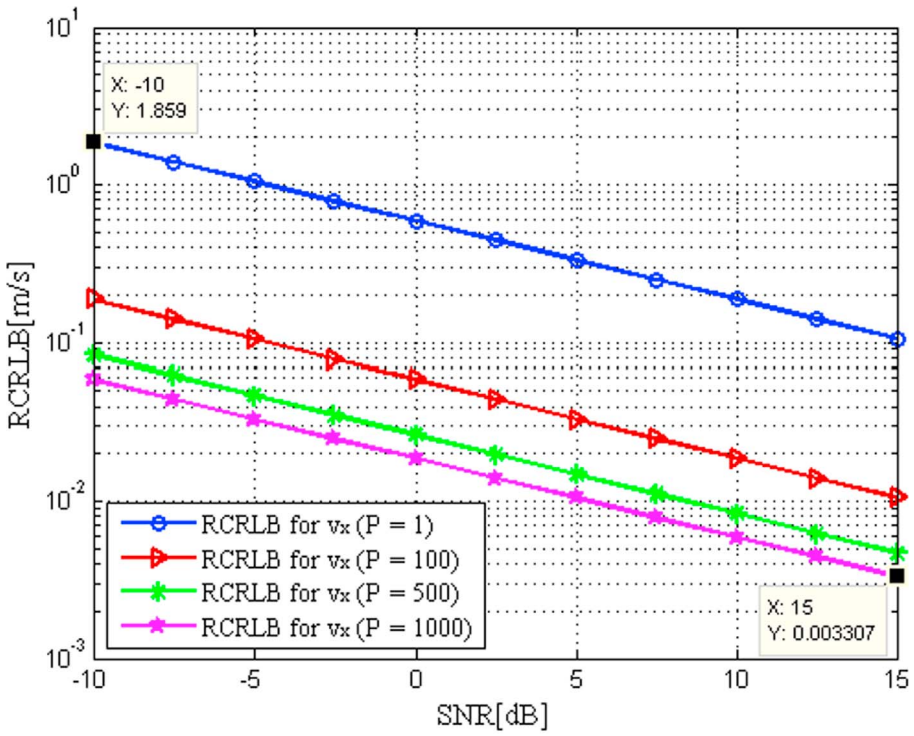

(a)

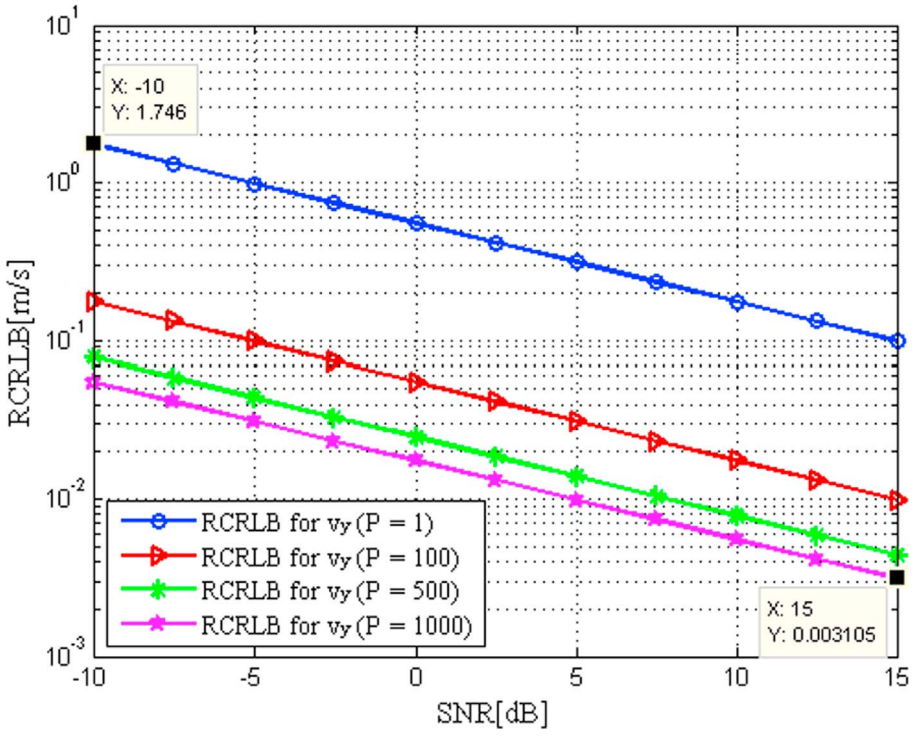

(b)

Figure 8. Square root of Cramér-Rao lower bound (RCRLB) in the target position dimensions versus signal-to-noise ratio (SNR) with different P when $T_0 = 1$ s and $\beta = 20$: (a) x position; (b) y position.

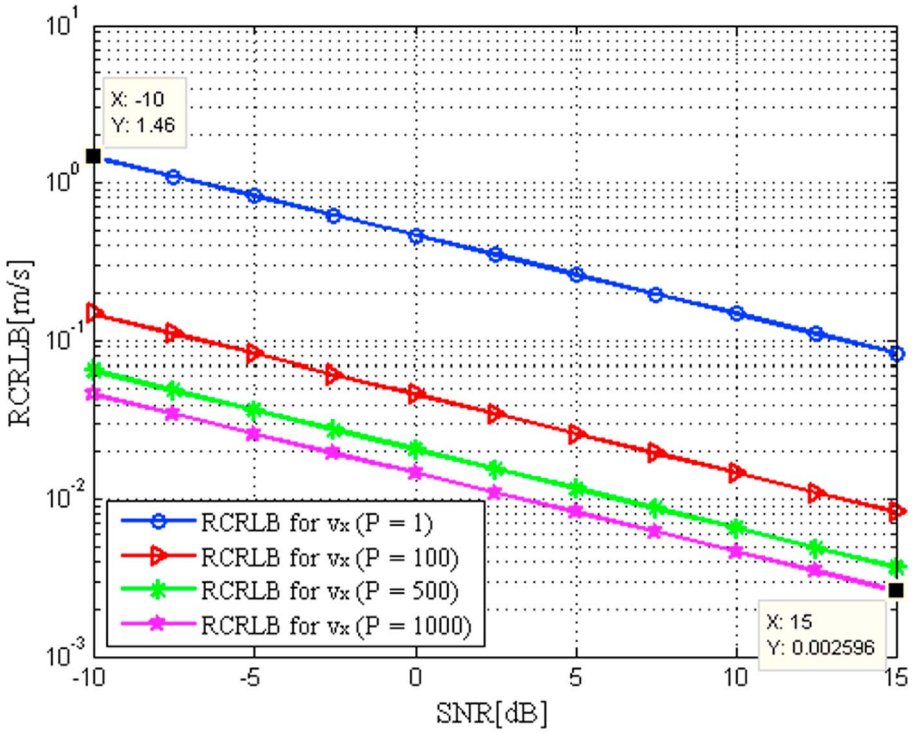

(a)

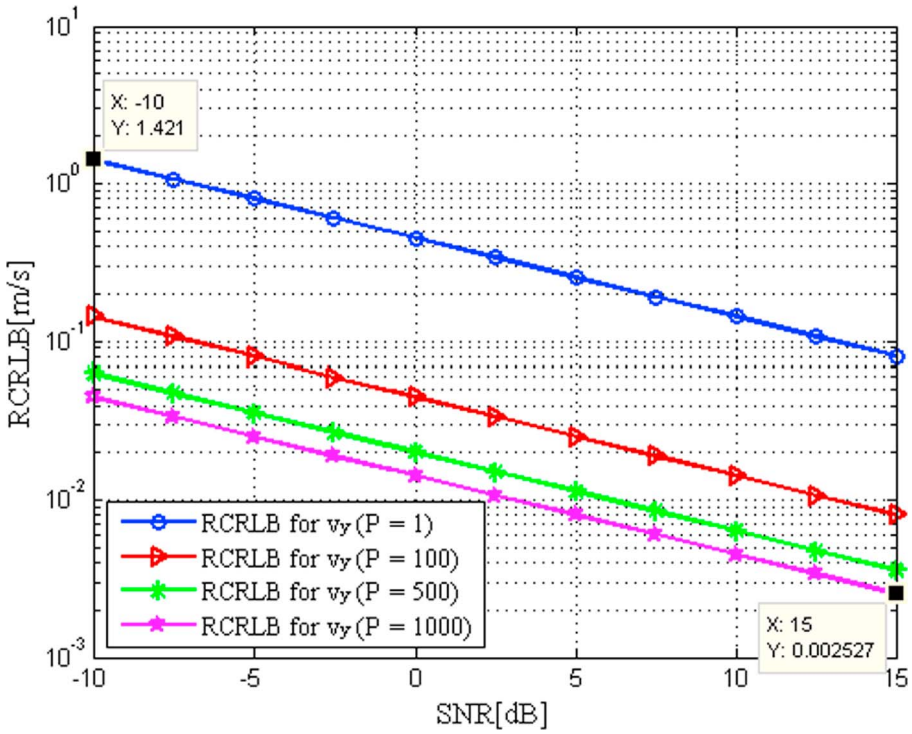

(b)

Figure 9. Square root of Cramér-Rao lower bound (RCRLB) in the target velocity dimensions versus signal-to-noise ratio (SNR) with different P when $T_0 = 1$ s and $\beta = 20$: (a) x velocity; (b) y velocity.

Moreover, in Figures 8 and 9, the RCRLBs for both target position and velocity estimates are plotted versus SNR for fixed $T_0 = 1$ s and $\beta = 20$, respectively. As expected, larger modulation index leads to wider signal bandwidth. From Figure 8, it is seen that the RCRLB becomes 0.03865 m for p_x and 0.04193 m for p_y when SNR = 15 dB and $P = 1{,}000$, which are much lower than those in Figure 6. The results in Figure 9 show the same trends compared with Figure 7, where the RCRLB at SNR=15 dB for v_x is 0.002596 m/s and that for v_y is 0.002527 m/s. Comparing the RCRLBs in Figures 6–9, we find that larger observation time T_0 and modulation index β are beneficial to improve the joint estimation accuracy of target position and velocity.

4.3. Discussion

The following can be concluded from the simulation results:

1. Grouping the receiving elements into properly sized arrays can reduce the mean square error of target parameter estimation (Khomchuk et al., 2016).
2. The joint CRLB is a function of SNR, the number of receiving antenna elements, the properties of the transmitted waveform such as observation time and modulation index, and the relative geometry between the target and the FM-based DPRN system.
3. The FM-based transmitted signals with larger observation time T_0 and modulation index β are beneficial to improve the estimation accuracy of target position and velocity. These results indicate that a waveform with a larger data set will achieve better estimation performance, which in turn will increase the data processing requirement (Javed et al., 2016).
4. The DPRN architectures have received increasing attention in the radar community owing to their advantages of low cost, low probability of intercept property, and so on. However, there are some nonnegligible drawbacks, such as nonoptimized waveforms, the low transmitted power levels, the broad antenna beams, and the high cochannel interferences (Anastasio et al., 2014). These drawbacks may imply a probability of detection in the range from 60% to 85% for acceptable probabilities of false alarm. Thus, the standard CRLB will be too optimistic for a realistic evaluation of the target parameter estimation performance. For this motivation, the CRLB with $P_d < 1$ for joint target parameter estimation accuracy in a DPRN will be derived in the future.

5. Conclusion

This paper investigated the joint estimation of the target position and velocity parameters for FM-based DPRN system with antenna arrays. The signal model we utilized had been developed for simplicity but was said to be accurate enough to give meaningful evaluations. The log-likelihood function of the received signal for a complex Gaussian extended target is analyzed. Then, the CRLB associated with the MLE method were derived to analyze the target parameter estimation performance. The simulation results showed that the estimation accuracy of the target parameters can be significantly improved with more receiving antenna elements. Finally, numerical simulations were presented to demonstrate that the joint CRLB depends not only on the geometry between the target and the DPRN system but also on the SNR value, the number of receiving antenna elements, and the transmitted FM waveform parameters such as observation time and modulation index.

It should be mentioned that the low probability of detection values make the target parameter estimation accuracy predicted by the standard CRLB too optimistic, which is due to the fact that the possibility of missing detections is neglected. Hence, a modified CRLB is required to provide a more realistic prediction of the target estimation performance. Future work will concentrate on the joint target parameter estimation performance with missing observations, namely, for the probability of detection $P_d < 1$.

Appendix A: The Elements of FIM $\mathbf{J}_{ij}(\boldsymbol{\Theta})$

The elements of the symmetric FIM $\mathbf{J}_{ij}(\boldsymbol{\mu})$ corresponding to the ijth transmitter-receiver pair are given by

$$J_{ij}^{11}(\boldsymbol{\mu}) = \frac{2\pi f \beta^2}{T_0}\left[2\pi f T_0 + \sin(2\pi f T_0)\cos(2\phi)\right]\left(\frac{\partial \tau_{ij}^{\mu}}{\partial p_x}\right)^2 + \frac{2\beta \sin(\phi)}{\pi f T_0}\left[\sin(\pi f T_0) - \pi f T_0 \cos(\pi f T_0)\right]\left(\frac{\partial \tau_{ij}^{\mu}}{\partial p_x}\right)\left(\frac{\partial f_{D_{ij}}^{\mu}}{\partial p_x}\right) + \frac{T_0^2}{12}\left(\frac{\partial f_{D_{ij}}^{\mu}}{\partial p_x}\right)^2, \tag{A1}$$

$$J_{ij}^{12}(\boldsymbol{\mu}) = J_{ij}^{21}(\boldsymbol{\mu}) = \left\{ \frac{2\pi f \beta^2}{T_0} \left[2\pi f T_0 + \sin(2\pi f T_0)\cos(2\phi) \right] \left(\frac{\partial \tau_{ij}^{\mu}}{\partial p_x} \right) + \frac{\beta \sin(\phi)}{\pi f T_0} \left[\sin(\pi f T_0) - \pi f T_0 \cos(\pi f T_0) \right] \left(\frac{\partial f_{D_{ij}}^{\mu}}{\partial p_x} \right) \right\} \left(\frac{\partial \tau_{ij}^{\mu}}{\partial p_y} \right) + \left\{ \frac{\beta \sin(\phi)}{\pi f T_0} \left[\sin(\pi f T_0) - \pi f T_0 \cos(\pi f T_0) \right] \left(\frac{\partial \tau_{ij}^{\mu}}{\partial p_x} \right) + \frac{T_0^2}{12} \left(\frac{\partial f_{D_{ij}}^{\mu}}{\partial p_x} \right) \right\} \left(\frac{\partial f_{D_{ij}}^{\mu}}{\partial p_y} \right), \tag{A2}$$

$$J_{ij}^{13}(\boldsymbol{\mu}) = J_{ij}^{31}(\boldsymbol{\mu}) = \left\{ \frac{\beta \sin(\phi)}{\pi f T_0} \left[\sin(\pi f T_0) - \pi f T_0 \cos(\pi f T_0) \right] \left(\frac{\partial \tau_{ij}^{\mu}}{\partial p_x} \right) + \frac{T_0^2}{12} \left(\frac{\partial f_{D_{ij}}^{\mu}}{\partial p_x} \right) \right\} \left(\frac{\partial f_{D_{ij}}^{\mu}}{\partial v_x} \right), \tag{A3}$$

$$J_{ij}^{14}(\boldsymbol{\mu}) = J_{ij}^{41}(\boldsymbol{\mu}) = \left\{ \frac{\beta \sin(\phi)}{\pi f T_0} \left[\sin(\pi f T_0) - \pi f T_0 \cos(\pi f T_0) \right] \left(\frac{\partial \tau_{ij}^{\mu}}{\partial p_x} \right) + \frac{T_0^2}{12} \left(\frac{\partial f_{D_{ij}}^{\mu}}{\partial p_x} \right) \right\} \left(\frac{\partial f_{D_{ij}}^{\mu}}{\partial v_y} \right), \tag{A4}$$

$$J_{ij}^{22}(\boldsymbol{\mu}) = \frac{2\pi f \beta^2}{T_0} \left[2\pi f T_0 + \sin(2\pi f T_0)\cos(2\phi) \right] \left(\frac{\partial \tau_{ij}^{\mu}}{\partial p_y} \right)^2 + \frac{2\beta \sin(\phi)}{\pi f T_0} \left[\sin(\pi f T_0) - \pi f T_0 \cos(\pi f T_0) \right] \left(\frac{\partial \tau_{ij}^{\mu}}{\partial y} \right) \left(\frac{\partial f_{D_{ij}}^{\mu}}{\partial p_y} \right) + \frac{T_0^2}{12} \left(\frac{\partial f_{D_{ij}}^{\mu}}{\partial p_y} \right)^2, \tag{A5}$$

$$J_{ij}^{23}(\boldsymbol{\mu}) = J_{ij}^{32}(\boldsymbol{\mu}) = \left\{ \frac{\beta \sin(\phi)}{\pi f T_0} \left[\sin(\pi f T_0) - \pi f T_0 \cos(\pi f T_0) \right] \left(\frac{\partial \tau_{ij}^{\mu}}{\partial p_y} \right) + \frac{T_0^2}{12} \left(\frac{\partial f_{D_{ij}}^{\mu}}{\partial p_y} \right) \right\} \left(\frac{\partial f_{D_{ij}}^{\mu}}{\partial v_x} \right), \tag{A6}$$

$$J_{ij}^{24}(\boldsymbol{\mu}) = J_{ij}^{42}(\boldsymbol{\mu}) = \left\{ \frac{\beta \sin(\phi)}{\pi f T_0} \left[\sin(\pi f T_0) - \pi f T_0 \cos(\pi f T_0) \right] \left(\frac{\partial \tau_{ij}^{\mu}}{\partial p_y} \right) + \frac{T_0^2}{12} \left(\frac{\partial f_{D_{ij}}^{\mu}}{\partial p_y} \right) \right\} \left(\frac{\partial f_{D_{ij}}^{\mu}}{\partial v_y} \right), \tag{A7}$$

$$J_{ij}^{33}(\boldsymbol{\mu}) = \frac{T_0^2}{12} \left(\frac{\partial f_{D_{ij}}^{\mu}}{\partial v_x} \right)^2, \tag{A8}$$

$$J_{ij}^{34}(\boldsymbol{\mu}) = J_{ij}^{43}(\boldsymbol{\mu}) = \frac{T_0^2}{12} \left(\frac{\partial f_{D_{ij}}^{\mu}}{\partial v_x} \right) \left(\frac{\partial f_{D_{ij}}^{\mu}}{\partial v_y} \right), \tag{A9}$$

$$J_{ij}^{44}(\boldsymbol{\mu}) = \frac{T_0^2}{12} \left(\frac{\partial f_{D_{ij}}^{\mu}}{\partial v_y} \right)^2. \tag{A10}$$

Acknowledgments

We note that there are no data-sharing issues since all of the numerical information is provided in the figures, which are realized by MATLAB software. The MATLAB programs and numerical data are available upon request to the first author (scg_space@163.com). This work is supported in part by the National Natural Science Foundation of China (grants 61371170 and 61671239), in part by the Fundamental Research Funds for the Central Universities (grants NS2016038 and NP2015404), in part by the National Aerospace Science Foundation of China (grant 20152052028), in part by the Priority Academic Program Development of Jiangsu Higher Education Institutions (PADA), and in part by Key Laboratory of Radar Imaging and Microwave Photonics (Nanjing University of Aeronautics and Astronautics), Ministry of Education, Nanjing University of Aeronautics and Astronautics, Nanjing, 210016, China.

References

Anastasio, V., Farina, A., Colone, F., & Lombardo, P. (2014). Cramér-Rao lower bound with $P_d < 1$ for target localisation accuracy in multistatic passive radar. *IET Radar, Sonar and Navigation*, *8*(7), 767–775.

Cheng, Z. Y., He, Z. S., & Zheng, X. J. (2016). CRB for joint estimation of moving target in distributed phased array radars on moving platforms. In *IEEE 13th International Conference on Signal Processing (ICSP)* (pp. 1461–1465). Chengdu, China.

D'Andrea, A. N., Mengali, U., & Reggiannini, R. (1994). The modified Cramer-Rao bound and its application to synchronization problems. *IEEE Transactions on Communications*, *42*(234), 1391–1399.

Daout, F., Schmitt, F., Ginolhac, G., & Fargette, P. (2012). Multistatic and multiple frequency imaging resolution analysis—Application to GPS-based multistatic radar. *IEEE Transactions on Aerospace and Electronic Systems*, *48*(4), 3042–3057.

Filip, A., & Shutin, D. (2016). Cramér-Rao bounds for L-band digital aeronautical communication system type 1 based passive multiple-input multiple-output radar. *IET Radar, Sonar & Navigation*, *10*(2), 348–358.

Fisher, E., Haimovich, A., Blum, R. S., Cimini, L. J., Chizhik, D., & Valenzuela, R. A. (2006). Spatial diversity in radars—Models and detection performance. *IEEE Transactions on Signal Processing*, *54*(3), 823–836.

Godrich, H., Haimovich, A. M., & Blum, R. S. (2010). Target localization accuracy gain in MIMO radar-based systems. *IEEE Transactions on Information Theory*, *56*(6), 2783–2803.

Godrich, H., Petropulu, A., & Poor, H. V. (2011). Power allocation strategies for target localization in distributed multiple-radar architectures. *IEEE Transactions on Signal Processing*, *59*(7), 3226–3240.
Gogineni, S., Rangaswamy, M., Rigling, B. D., & Nehorai, A. (2014). Cramér-Rao bounds for UMTS-based passive multistatic radar. *IEEE Transactions on Signal Processing*, *62*(1), 95–106.
Greco, M. S., Stinco, P., Gini, F., & Farina, A. (2011). Cramer-Rao bounds and selection of bistatic channels for multistatic radar systems. *IEEE Transactions on Aerospace and Electronic Systems*, *47*(4), 2934–2948.
Hack, D. E., Patton, L. K., Himed, B., & Saville, M. A. (2014). Detection in passive MIMO radar networks. *IEEE Transactions on Signal Processing*, *62*(11), 2999–3012.
Haimovich, A. M., Blum, R. S., & Cimini, L. J. Jr. (2008). MIMO radar with widely separated antennas. *IEEE Signal Processing Magazine*, *25*(1), 116–129.
He, Q., Blum, R. S., & Haimovich, A. M. (2010). Noncoherent MIMO radar for location and velocity estimation: More antennas means better performance. *IEEE Transactions on Signal Processing*, *58*(7), 3661–3680.
He, Q., Blum, R. S., Rodrich, H., & Haimovich, A. M. (2010). Target velocity estimation and antenna placement for MIMO radar with widely separated antennas. *IEEE Journal of Selected Topics on Signal Processing*, *4*(1), 79–100.
He, Q., Hu, J. B., Blum, R. S., & Wu, Y. (2016). Generalized Cramér-Rao bound for joint estimation of target position and velocity for active and passive radar networks. *IEEE Transactions on Signal Processing*, *64*(8), 2078–2089.
Hu, J. B., Li, M., He, Q., He, Z., & Blum, R. S. (2017). Joint estimation of MIMO-OTH radar measurements and ionospheric parameters. *IEEE Transactions on Aerospace and Electronic Systems*, *53*(6), 2789–2805.
Javed, M. N., Ali, S., & Hassan, S. A. (2016). 3D MCRLB evaluation of a UMTS-based passive multistatic radar operating in a line-of-sight environment. *IEEE Transactions on Signal Processing*, *64*(19), 5131–5144.
Kalkan, Y. (2013). Cramer-Rao bounds for target position and velocity estimations for widely separated MIMO radar. *Radioengineering*, *22*(4), 1156–1161.
Khomchuk, P., Blum, R. S., & Bilik, I. (2016). Performance analysis of target parameters estimation using multiple widely separated antenna arrays. *IEEE Transactions on Aerospace and Electronic Systems*, *52*(5), 2413–2435.
Li, J., & Stoica, P. (2007). MIMO radar with colocated antennas. *IEEE Signal Processing Magazine*, *24*(5), 106–114.
Li, J., & Stoica, P. (2009). *MIMO radar signal processing*. Hoboken, NJ: Wiley.
Li, N. J. (1995). Radar ECCMs new area: Anti-stealth and anti-ARM. *IEEE Transactions on Aerospace and Electronic Systems*, *31*(3), 1120–1127.
Naghsh, M. M., Mahmoud, M. H., Shahram, S. P., Mojtaba, S., & Petre, S. (2013). Unified optimization framework for multi-static radar code design using information-theoretic criteria. *IEEE Transactions on Signal Processing*, *61*(21), 5401–5416.
Niu, R. X., Blum, R. S., Varshney, P. K., & Drozd, A. L. (2012). Target localization and tracking in noncoherent multiple-input multiple-output radar systems. *IEEE Transactions on Aerospace and Electronic Systems*, *48*(2), 1466–1489.
Pace, P. E. (2009). *Detecting and classifying low probability of intercept radar*. Boston: Artech House.
Shi, C. G., Salous, S., Wang, F., & Zhou, J. (2016a). Cramer-Rao lower bound evaluation for linear frequency modulation based active radar networks operating in a Rice fading environment. *Sensors*, *16*(12), 1–17.
Shi, C. G., Salous, S., Wang, F., & Zhou, J. J. (2016b). Modified Cramér-Rao lower bounds for joint position and velocity estimation of a Rician target in OFDM-based passive radar networks. *Radio Science*, *52*, 15–33. https://doi.org/10.1002/2016RS006158
Shi, C. G., Salous, S., Wang, F., & Zhou, J. J. (2017). Power allocation for target detection in radar networks based on low probability of intercept: A cooperative game theoretical strategy. *Radio Science*, *52*, 1030–1045. https://doi.org/10.1002/2017RS006332
Shi, C. G., Wang, F., Salous, S., & Zhou, J. (2017). Performance analysis for joint target parameter estimation in UMTS-based passive multistatic radar with antenna arrays using modified Cramér-Rao lower bounds. *Sensors*, *17*, 2379. https://doi.org/10.3390/s17102379
Shi, C. G., Wang, F., Sellathurai, M., & Zhou, J. (2016). Transmitter subset selection in FM-based passive radar networks for joint target parameter estimation. *IEEE Sensors Journal*, *16*(15), 6043–6052.
Shi, C. G., Wang, F., Sellathurai, M., Zhou, J., & Salous, S. (2017). Power minimization based robust OFDM radar waveform design for radar and communication systems in coexistence. *IEEE Transactions on Signal Processing*, *66*(5), 1316–1330. https://doi.org/10.1109/TSP.2017.2770086
Shi, C. G., Wang, F., Zhou, J. J., & Zhang, H. (2015). Security information factor based low probability of identification in distributed multiple-radar system. In *2015 IEEE International Conference on Acoustics, Speech and Signal Processing (ICASSP)* (pp. 3716–3720). Brisbane, QLD, Australia.
Shi, C. G., Wang, F., & Zhou, J. J. (2016). Cramér-Rao bound analysis for joint target location and velocity estimation in FM-based passive radar networks. *IET Signal Processing*, *10*(7), 70–80.
Shi, C. G., Zhou, J. J., & Wang, F. (2016). LPI based resource management for target tracking in distributed radar network. In *2016 IEEE Radar Conference (RadarConf)* (pp. 822–826). Philadelphia, PA.
Wei, C., He, Q., & Blum, R. S. (2010). Cramér-Rao bounds for joint location and velocity estimation in multi-target non-coherent MIMO radars. In *2010 44th IEEE Annual Conference on Information Sciences and Systems (CISS)* (pp. 1–6). Princeton, NJ.
Xie, R., Wan, X. R., Hong, S., & Yi, J. (2017). Joint optimization of receiver placement and illuminator selection for a multiband passive radar network. *Sensors*, *17*(6), 1–20.
Zaimbashi, A. (2017). Target detection in analog terrestrial TV-based passive radar sensor: Joint delay-Doppler estimation. *IEEE Sensors Journal*, *17*(17), 5569–5580.
Zhang, Z. K., Salous, S., Li, H. L., & Tian, Y. (2015). Optimal coordination method of opportunistic array radars for multi-target-tracking-based radio frequency stealth in clutter. *Radio Science*, *50*, 1187–1196. https://doi.org/10.1002/2015RS005728
Zhang, Z. K., & Tian, Y. B. (2016). A novel resource scheduling method of netted radars based on Markov decision process during target tracking in clutter. *EURASIP Journal on Advances in Signal Processing*, *2016*(16), 1–9.
Zhao, T., & Huang, T. Y. (2016). Cramér-Rao lower bounds for the joint delay-Doppler estimation of an extended target. *IEEE Transactions on Signal Processing*, *64*(6), 1562–1573.